Thermal Effects on Pull-Off Force in the Johnson–Kendall–Roberts Model

Yunong Zhou[1]

Abstract

In this study, we investigate the effects of thermal fluctuations on the generalized Johnson–Kendall–Roberts (JKR) model. We show that the distribution of pull-off forces in this model is similar to that of the Bradley model, and is also consistent with the experiment result observed in Wierez-Kien et al. (Nanotechnology 29(15):155704 2018). Increasing temperature leads to a broadening of the distribution, while leads to a reduction of the pull-off force. Additionally, the pull-off force, which is separated into an athermal term and a thermal-induced reduction term, is measured by using spring velocity ranging over 5 orders of magnitude. We show that for compliant spring, the pull-off force is significantly enhanced with increasing velocity, which is mainly attributed to the contribution of the thermal-induced reduction term, while the athermal term is barely sensitive to changes in velocity.

1 Introduction

Adhesion plays an important role in contact mechanics at different scales, such as the adhesive ability of natural insects on vertical walls [2, 3], and microelectromechanical systems [4]. As a simple and commonly used approach to adhesive contact mechanics in the Hertzian geometry, the Bradley model assumes that the interaction between the counterfaces is nothing but a Lennard-Jones (LJ) potential [5, 6]. In such a way, assuming that the surface energy is γ, and the radius of curvature is R, the pull-off force in athermal case estimated by this model is $2\pi\gamma R$, which is identical to the estimation of that in the Derjaguin-Muller-Toporov (DMT) model [7].

While it has been demonstrated several times that the DMT model is accurate in the limit of the long-range adhesion and stiff material [8–10], this model becomes increasingly inaccurate for large and soft matter, hence different assumptions on the interaction have led to the JKR model [11], in which a singular crack term is assumed near the contact line.

The thermal fluctuation, which is often ignored in most theoretical and numerical studies on contact mechanics, has been demonstrated several times in experiments that can lead to a noticeable reduction of pull-off force [1, 12]. In fact, it has been shown that thermal fluctuations limit the adhesive strength of compliant solids [13]. Therefore, modelling the thermal effects on pull-off force within the framework of JKR model would be worthwhile.

Additionally, in athermal case, the elastic body jumps out of contact when the spring stiffness k is less than the maximum curvature of the potential energy V''_{max}. This mechanism is analogous to that of the friction-velocity relation in the Prandtl model [14–16], in which a particle of mass m is dragged through a sinusoidal potential with a driving spring with velocity v. On the other hand, several experimental studies have demonstrated that the velocity can significantly affect the pull-off force [17–19]. In light of this fact, we expect that this model to also accurately describe the relation between pull-off force and velocity and further predict the contribution of thermal effects on this relation.

In this study, we set up a loading-unloading experiment *in silico*, in which a parabolic indenter is fixed in space, a linearly elastic body is placed below the indenter and is connected with an elastic spring, as shown in the inset of Fig. 1. This spring is used to characterize the stiffness of the cantilever and is allowed to move up and down with a

✉ Yunong Zhou
   yunong.zhou@uni-saarland.de

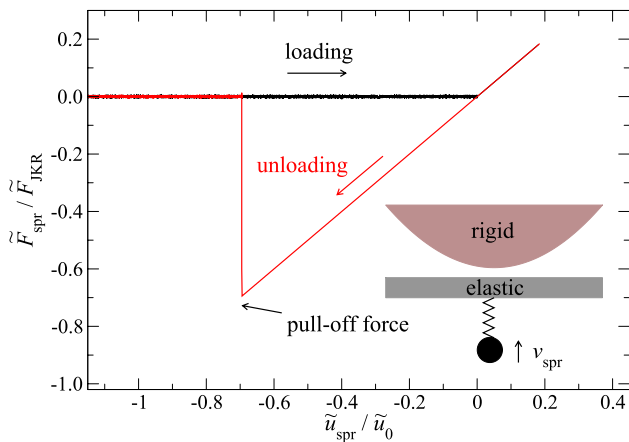1   Department of Materials Science and Engineering, Saarland University, 66123 Saarbrücken, Germany

Fig. 1 The reduced spring force $\tilde{F}_{\text{spr}}/\tilde{F}_{\text{JKR}}$ as a function of the reduced spring displacement $\tilde{u}_{\text{spr}}/\tilde{u}_0$, where $\tilde{u}_0$ represents the spring displacement at the pull-off point in athermal case, $\tilde{F}_{\text{JKR}} = 3\pi\tilde{\gamma}/2$ is the reduced pull-off force in athermal case. Inset shows the schematic illustration of a tip-substrate model for loading-unloading simulations

constant velocity [20]. The effects of thermal fluctuations can be cast as random forces, which have to satisfy the fluctuation-dissipation theorem (FDT) [21].

The first intention of this study is to validate whether this modified Bradley model can plausibly reproduce the experimental pull-off force distribution. Another intention is to explore the effect of spring velocity on the pull-off force. To discriminate the athermal pull-off force from the thermal pull-off force, the short-hand notation F_0 will be used to indicate the pull-off force in athermal case.

The remainder of this paper is organized as follows: Model and method are introduced in Sect. 2. results are presented in Sect. 3, while conclusions are drawn in Sect. 4.

2 Model and method

2.1 Modified Bradley model

In this model, the Newton's equation of motion of the elastic solid reads

$$m\ddot{u}_{\text{ela}} + m\eta(v_{\text{ela}} - v_{\text{spr}}) = -\frac{\partial V_{\text{tot}}}{\partial u_{\text{ela}}} + \Gamma(t), \tag{1}$$

where

$$V_{\text{tot}} = \frac{1}{2}k(u_{\text{spr}} - u_{\text{ela}})^2 - \int_0^{u_{\text{ela}}} du F_{\text{cont}}, \tag{2}$$

m is the mass, η is the damping coefficient, k the stiffness of the driving spring, u_{ela} and u_{spr} represent the displacement of elastic body and driving spring, respectively. $\Gamma(t)$ is a random force characterizing the thermal fluctuations

and thus must satisfy the FDT. F_{cont} represents the contact force within the framework of JKR model, which can be determined by

$$F_{\text{cont}} = \frac{4E^*}{3R}a_{\text{c}}^3 - \sqrt{8\pi\gamma E^*}a_{\text{c}}^{3/2} \tag{3}$$

$$u_{\text{ela}} = \frac{a_{\text{c}}^2}{R} - \sqrt{\frac{2\pi\gamma}{E^*}}a_{\text{c}}^{1/2} \tag{4}$$

jointly, where E^* is the contact modulus and a_{c} the contact area [22]. The pull-off force in athermal case is given by $F_{\text{JKR}} = 3\pi\gamma R/2$.

To eliminate the effect of different unit systems, the model should be expressed in a reduced system in which η, R and E^* as well as k_B are equal to unity. Therefore, the remaining reduced parameters in this model are reduced mass $\tilde{m} = m\eta^2/(E^*R)$, reduced velocity $\tilde{v} = v/(R\eta)$, reduced stiffness $\tilde{k} = k/(E^*R)$, reduced thermal energy $k_B\tilde{T} = k_BT/(E^*R^3)$ and reduced surface energy $\tilde{\gamma} = \gamma/(E^*R)$. These five independent, dimensional variables can fully determine the performance of this model.

2.2 Simulation method

In molecular dynamics simulation, we apply velocity Verlet algorithm to propagate the equation of motion in Eq. (1), which is a typical Langevin dynamics (LD). The random forces, which are used to characterize the thermal fluctuations, as mentioned before, must satisfy the FDT, which means, the mean and second moment of random forces must obey

$$\langle \Gamma(t) \rangle = 0 \tag{5}$$

$$\langle \Gamma(t)\Gamma(t') \rangle = 2m\eta k_B T\delta(t - t') \tag{6}$$

respectively, where $\langle \cdot \rangle$ represents ensemble average and $\delta(\cdot)$ denotes the Dirac delta function.

In a certain simulation, the random forces are realized by

$$\Gamma_\tau = \sqrt{\frac{6m\eta k_B T}{\Delta t}}(2u_\tau - 1) \tag{7}$$

where u_τ is a (pseudo) random number generator, which can produce random numbers uniformly distributed between [0, 1], Δt is time step and τ is an integer to account the time step. In such a way, the random forces will satisfy the FDT automatically.

Now we must specify the time step Δt. Towards this end, we first determine the value of the mass m, which must be well chosen so that the dynamics is slightly underdamped, specifically, it equals to $m = 4V_{\text{tot}}''/\eta^2$. The time step, on one hand, should be fairly small compared

to the system period, which is given by $2\pi\sqrt{m/V''_{tot}}$. On the other hand, it should be small compared to the retract period, which is given by u_c/v_{spr}, where u_c is the distance from unloading position to the jump-out-of-contact position. The expression of u_c can be determined by Eqs. (3-4) jointly. Therefore, the time step used in our simulation can be written as below,

$$\Delta t = \frac{1}{40}\min\left\{2\pi\sqrt{\frac{m}{V''_{tot}}}, \frac{u_c}{v_{spr}}\right\}. \tag{8}$$

Additionally, the random forces should be separated into two parts, which reads

$$\Gamma(t) = \Gamma_{ela}(t) + \Gamma_{cont}(t) \tag{9}$$

where Γ_{ela} is used to simulate the thermal effects on the driving spring, which indicates that it exists throughout the simulation, while Γ_{cont} is used to characterize the thermal effects when the elastic body jumps into contact, which follows the spirit of assumptions in the JKR model.

In real experiments, the interaction between the counterfaces results in the vertical deflection of the cantilever. Therefore, the applied force can be deduced from the deflection according to the Hooke's law [23, 24]. In light of this fact, we measure the spring force F_{spr} in simulations, which is given by

$$\tilde{F}_{spr} = -\tilde{k}\left(\tilde{u}_{spr} - \tilde{u}_{ela}\right) \tag{10}$$

On the other hand, considering that the Langevin dynamics will become inefficient in the case of over-damped simulation as the time step of the simulation Δt should be very small compared to the damping time $1/\eta$. This fact motivates us to employ the Brownian dynamics (BD), which can be described as a special case of the Langevin dynamics, that is, the inertia $m\ddot{u}_{ela}$ presented in Eq. (1) equals to zero. This allows the Eq. (1) to be reduced to

$$0 = -\frac{\partial V_{tot}}{\partial u_{ela}} - m\eta\left(v_{ela} - v_{spr}\right) + \Gamma(t). \tag{11}$$

The equation of motion applied for Brownian dynamics can also be achieved by assuming that the mass m is infinitely small while $m\eta$ is fixed to non-zero, which corresponds to the over-damped Langevin dynamics. To propagate the simulation, the velocity of the elastic body can be approximated as $v_{ela} = (u_{ela}^{now} - u_{ela}^{old})/\Delta t$, as a result, we can write

$$u_{ela}^{now} = u_{ela}^{old} + \frac{\Delta t}{m\eta}[m\eta v_{spr} - \frac{\partial V_{tot}}{\partial u_{ela}} + \Gamma(t)], \tag{12}$$

the time step is chosen as $\Delta t = 1/(20\eta)$ so that it is fairly small compared to the damping time.

3 Results

3.1 Distribution of pull-off forces

In this section, we address the question how thermal fluctuations affect the distribution of pull-off force. As a first glance, Fig. 1 shows a force-displacement hysteresis of a single loading-unloading simulation considering the JKR force and the thermal effects. The reduced parameters which matter this simulation are chosen as $\tilde{m} = 5.0 \times 10^{-5}$, $\tilde{v}_{spr} = 1.0 \times 10^{-4}$, $\tilde{k} = 2.0 \times 10^{-5}$, $k_B\tilde{T} = 5.0 \times 10^{-8}$ and $\tilde{\gamma} = 1.2 \times 10^{-4}$.

In this single loading-unloading hysteresis, it is interesting to observe that the pull-off force is significantly reduced. We would suggest that the adhesive strength is limited in value by thermal fluctuations, which had been noted by Tang *et.al* [13].

To further study how thermal fluctuations affect the pull-off force, we should firstly demonstrate if our simulation can reasonably reflect the real experiment. Towards this end, we measured the distribution of pull-off force from a mass of loading-unloading simulations, the parameters are well chosen so that they are approximately of the same order as those used in real experiments, which is also applied to simulate the single loading-unloading hysteresis in Fig. 1.

With the choice of parameters, we can map these reduced units to real units, it could be conducted by assuming that $E^* \approx 20.0$ GPa and $R \approx 15.7$ nm. The associated parameters with real unit are $\gamma = 3.6 \times 10^{-2}$ J/m², $k = 6.3 \times 10^{-3}$ N/m and $T = 288.4$ K. Furthermore, we assume that the mass $m \approx 1.0 \times 10^{-12}$ kg, which is of the same order as applied in several experimental studies on atomic force microscopy (AFM) contact problems [12, 25], thus it turns out to be a reasonable choice and the resulting velocity of the driving spring is $v_{spr} = 196.3$ nm/s.

It should be mentioned that this set of parameters implies that our simulations are most relevant at least in the case of weak interactions, that is, in the case where van der Waals interactions are the only forces at work between the interfaces [26, 27].

The result is shown in Fig. 2, which is obtained from more than 2000 loading-unloading simulations. To map our simulation to real experiment, this figure is plotted with real units rather than reduced units. The data presented in this figure reveals a good agreement between simulation and the experiment reported in Ref. [1], which follows an asymmetric bell-like curve.

Figure 3 shows reduced pull-off force distributions with different temperatures. The distribution depicted in Fig. 2 is applied as the reference data, while the real units are replaced by reduced units. It indicates that the pull-off
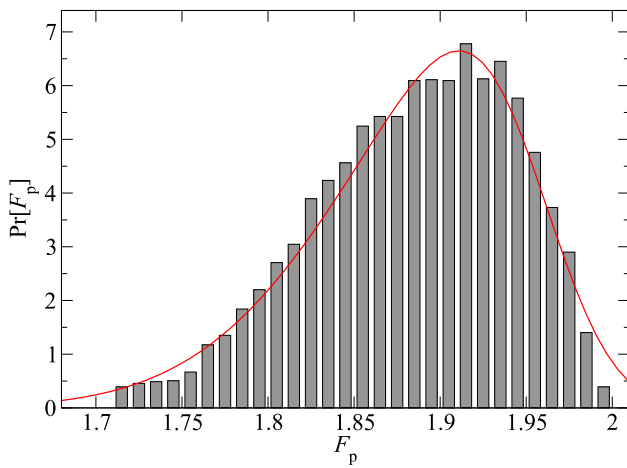
Fig. 2 Comparison of experimental data and simulation data on pull-off force distribution. The experimental distribution (grey bars) is obtained from the Fig. 5 of Ref. [1], while the data is renormalized so that the integration equals to unity. The simulation data (red line) is obtained from the method introduced in this study
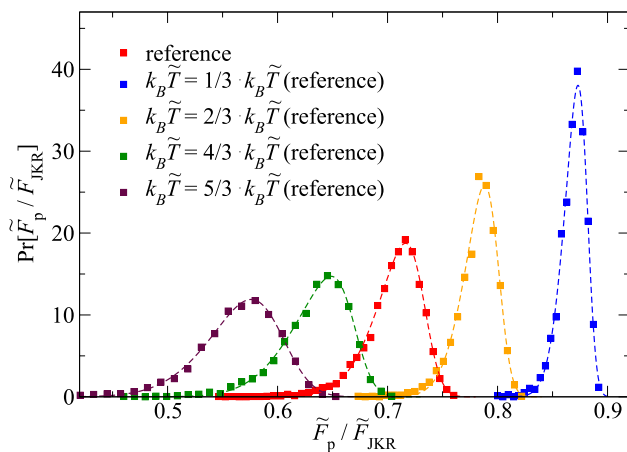

Fig. 3 Normalized pull-off force distribution with various temperatures. Solid squares represent the simulation results while dashed lines represent fitting curves using the skew-Gaussian probability density function. All pull-off force distributions are obtained from more than 2000 simulations

force distributions can be fitted reasonably well with the probability density function of skew-Gaussian distribution. Additionally, it confirms that the pull-off force decreases with increasing temperature. Similar results are also observed in the Bradley model simulations by Pinon *et al.* [12].

3.2 Relation between pull-off forces and velocity

In this section, we investigate how velocity of the driving spring $\tilde{v}_{spr}$ affects the pull-off force $\tilde{F}_p$. Towards this end, both Brownian dynamics and Langevin dynamics are

performed to measure the pull-off force with velocity ranging over 5 orders of magnitude at various temperatures. In both dynamics, η, E^* and R as well as k_B are fixed to unity. The reduced surface energy $\tilde{\gamma}$ is well chosen such that the depth of the JKR potential equals to unity, which leads to $\tilde{\gamma} \approx 0.229$.

In terms of the reduced mass, two cases are considered. In one case, it is set to infinity, while the $m\eta$ is fixed, which leads to overdamped simulation or Brownian dynamics. In another case, the value of the reduced mass is determined such that the simulation is slightly underdamped, in this study, it is fixed to $\tilde{m} = 0.01$.

To project the simulations to practical experiments, it is important to map the reduced units to real units. Towards this end, we assume that the contact modulus $E^* = 1$ GPa, the radius of curvature $R = 16$ nm and the mass $m \approx 10^{-12}$ kg as used in Ref. [12, 25] is nevertheless a reasonable choice. This makes the velocity v_{spr} be roughly located in the range 64 nm/s $\le v_{spr} \le 3.2$ mm/s, and the velocities used by indenters in several AFM loading-unloading experiments also fall in this range [17, 28].

Since this study considers the effects of thermal fluctuations on pull-off force, it is expected to separate the pull-off force into two parts, which reads,

$$\tilde{F}_p(\tilde{v}_{spr}, k_B\tilde{T}) = \tilde{F}_0(\tilde{v}_{spr}, 0) - \tilde{F}_t(\tilde{v}_{spr}, k_B\tilde{T}) \tag{13}$$

where $\tilde{F}_0$ is the pull-off force in athermal case, while $\tilde{F}_t$ represents the thermal-induced reduction on pull-off force.

Figure 4 compares Brownian and Langevin dynamics for various spring stiffness at athermal case. $\tilde{F}_0(v_{spr})$ relation differs noticeably at large velocity for underdamped and overdamped simulations. Nevertheless, both simulations show similar trend, that is, $\tilde{F}_0(v_{spr})$ is enhanced with increasing
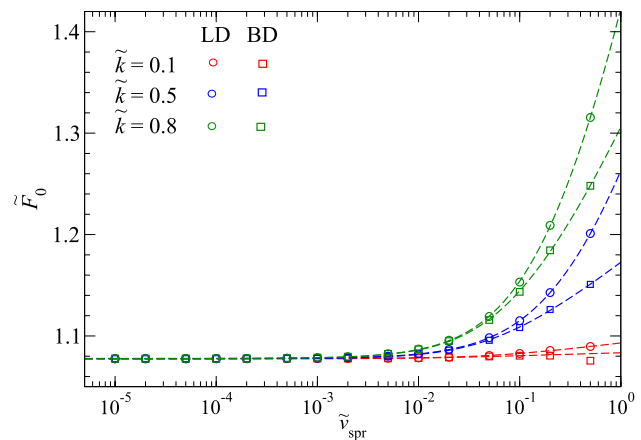

Fig. 4 Reduced athermal pull-off force $\tilde{F}_0$ as a function of velocity $\tilde{v}_{spr}$ for Brownian and Langevin dynamics respectively at different spring stiffness. Open symbols represent the dynamics while dashed lines represent the fitting curves

velocity, and it can be fit very well over an extended velocity range $10^{-5} \leq \tilde{v}_{spr} \leq 0.5$ with expression

$$\tilde{F}_0(\tilde{v}_{spr}, 0) = \tilde{F}_{JKR} \left\{ 1 + \left(\frac{\tilde{v}_{spr}}{v_0} \right)^{\alpha_0} \right\}^{\beta_0}, \qquad (14)$$

where v_0, α_0 and β_0 are dimensionless parameters.

Furthermore, it is interesting to note that the exponent β_0 is remarkably reduced from 0.134 to 0.005 when $\tilde{k}$ is decreased from 0.8 to 0.1 for Langevin dynamics, similar reduction is also observed for Brownian dynamics. This implies that for compliant spring, the velocity can barely affect the athermal pull-off force $\tilde{F}_0$. In practical AFM loading-unloading curve, a compliant spring is generally applied to identify the pull-off force in order to obtain precise results [29–31]. Therefore, it is more attractive to identify how velocity affects the pull-off force in the case of compliant spring.

Figures 5 and 6 show how velocity $\tilde{v}_{spr}$ affects the thermal-induced reduction on pull-off force $\tilde{F}_t$ for $\tilde{k} = 0.1$ in Langevin and Brownian dynamics respectively. All simulations are performed in an extended velocity range $10^{-5} \leq \tilde{v}_{spr} \leq 0.5$ and can be fitted very well with expression

$$\tilde{F}_t(\tilde{v}_{spr}, k_B\tilde{T}) = \xi \left\{ 1 + \alpha_t \exp \left[-\left(\frac{\tilde{v}_{spr}}{v_t} \right)^{\beta_t} \right] \right\}, \qquad (15)$$

where ξ, v_t, α_t and β_t are dimensionless parameters which varies with different temperatures.

When $\tilde{v}_{spr}$ is increased, the reduction of pull-off force is noticeably decreased, which as a result leads to an increment of the pull-off force $\tilde{F}_p$. In addition, when $\tilde{k} = 0.1$, the velocity dependence of athermal pull-off force $\tilde{F}_0(\tilde{v}_{spr})$ is quite
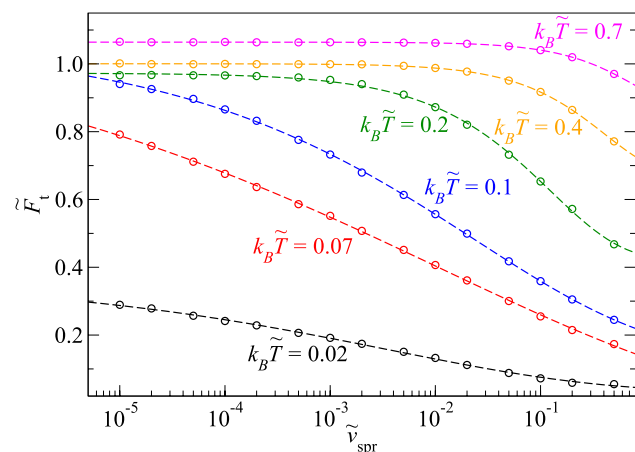
Fig. 6 Thermal-induced reduction of pull-off force $\tilde{F}_t$ as a function of velocity $\tilde{v}_{spr}$ for Brownian dynamics at various temperatures. Lines are fits according to the fitting function as given in Eq. (15). The spring stiffness is fixed to $\tilde{k} = 0.1$
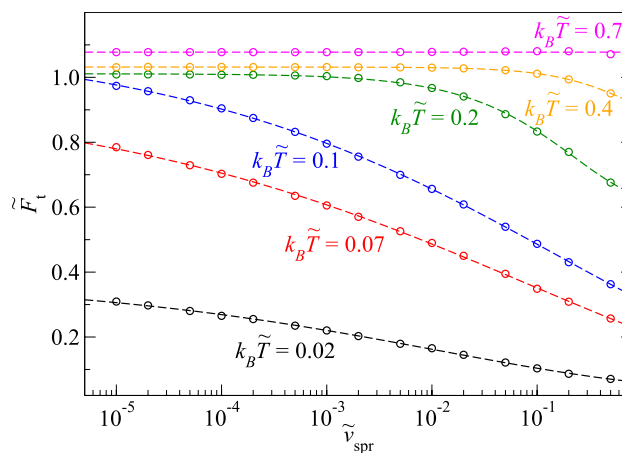
weak as the exponent β_0 is extremely small, which indicates that the increment in pull-off force is principally attributes to the effects of the thermal fluctuations.

It can also be observed in these two figures that with increasing temperature, the thermal-induced reduction in pull-off force will approach the athermal pull-off force and eventually cancels it out.

4 Conclusions

In this study, a modified Bradley model, in which the LJ interaction was replaced by the JKR contact force, was presented to study how thermal fluctuations affect the pull-off force. It was demonstrated that this model reasonably reproduced real AFM loading-unloading curve. At a given temperature, a skewed pull-off force distribution was observed by collecting a large number of simulation results. With appropriate parameters, the simulated distribution can be in plausible agreement with the experimental results, and can be fitted reasonably well with the skew Gaussian distribution. Increasing temperature leads to a reduction on pull-off force while a broadening of the distribution.

We also investigated the relation between pull-off force and the driving spring velocity when the thermal effects are considered. Towards this end, the pull-off force was separated into two contributions, namely, the athermal pull-off force and the thermal-induced reduction on pull-off force. When the value of the spring stiffness is fairly small, the athermal pull-off force has a weak dependence on velocity, in which case the thermal-induced reduction term dominate the velocity dependence of pull-off force. It is also observed

Fig. 5 Thermal-induced reduction of pull-off force $\tilde{F}_t$ as a function of velocity $\tilde{v}_{spr}$ for Langevin dynamics at various temperatures. Lines are fits according to the fitting function as given in Eq. (15). The spring stiffness is fixed to $\tilde{k} = 0.1$

that the pull-off force decreases as the temperature increases. The main reason for this reduction is that the increase in temperature leads to an enhancement in the value of thermal-induced reduction.

Compliance with ethical standards

Conflicts of interest The authors declare that they have no conflict of interest.

References

1. Wierez-Kien, M., Craciun, A.D., Pinon, A.V., Roux, S.L., Gallani, J.L., Rastei, M.V.: Interface bonding in silicon oxide nanocontacts: interaction potentials and force measurements. Nanotechnology **29**(15), 155704 (2018)
2. Boesel, L.F., Greiner, C., Arzt, E., del Campo, A.: Gecko-inspired surfaces: a path to strong and reversible dry adhesives. Adv. Mater. **22**(19), 2125 (2010)
3. Kim, S., Spenko, M., Trujillo, S., Heyneman, B., Santos, D., Cutkosky, M.: Smooth vertical surface climbing with directional adhesion. IEEE Trans. Rob. **24**(1), 65 (2008)
4. Zhao, Y.P., Wang, L.S., Yu, T.X.: Mechanics of adhesion in MEMS—a review. J. Adhes. Sci. Technol. **17**(3), 519 (2003)
5. Bradley, R.: LXXIX. The cohesive force between solid surfaces and the surface energy of solids. Philosoph. Mag. J. Sci. **13**(86), 853 (1932)
6. Gao, H., Wang, X., Yao, H., Gorb, S., Arzt, E.: Mechanics of hierarchical adhesion structures of geckos. Mech. Mater. **37**(2–3), 275 (2005)
7. Derjaguin, B., Muller, V., Toporov, Y.: Effect of contact deformations on the adhesion of particles. J. Colloid Interface Sci. **53**(2), 314 (1975)
8. Grierson, D.S., Flater, E.E., Carpick, R.W.: Accounting for the JKR–DMT transition in adhesion and friction measurements with atomic force microscopy. J. Adhes. Sci. Technol. **19**(3–5), 291 (2005)
9. Pashley, M.: Further consideration of the DMT model for elastic contact. Colloids Surf. **12**, 69 (1984)
10. Prokopovich, P., Perni, S.: Comparison of JKR- and DMT-based multi-asperity adhesion model: theory and experiment. Colloids Surf. A **383**(1–3), 95 (2011)
11. Johnson, K.L., Kendall, K., Roberts, A.: Surface energy and the contact of elastic solids. Proc. R Soc. Lond. Math. Phys. Sci. **324**(1558), 301 (1971)
12. Pinon, A.V., Wierez-Kien, M., Craciun, A.D., Beyer, N., Gallani, J.L., Rastei, M.V.: Thermal effects on van der Waals adhesive forces. Phys. Rev. B **93**, 3 (2016)
13. Tang, T., Jagota, A., Chaudhury, M.K., Hui, C.Y.: Thermal fluctuations limit the adhesive strength of compliant solids. J. Adhesion **82**(7), 671 (2006)
14. Prandtl, L.: Ein Gedankenmodell zur kinetischen Theorie der festen Körper. ZAMM Z. Angew. Math. Mech. **8**(2), 85 (1928)
15. Müser, M.H.: Velocity dependence of kinetic friction in the Prandtl-Tomlinson model. Phys. Rev. B **84**, 12 (2011)
16. Müser, M.H.: Shear thinning in the Prandtl model and its relation to generalized Newtonian fluids. Lubricants **8**(4), 38 (2020)
17. Xu, Q., Li, M., Niu, J., Xia, Z.: Dynamic enhancement in adhesion forces of microparticles on substrates. Langmuir **29**(45), 13743 (2013)
18. Xu, Q., Wan, Y., Hu, T.S., Liu, T.X., Tao, D., Niewiarowski, P.H., Tian, Y., Liu, Y., Dai, L., Yang, Y., Xia, Z.: Robust self-cleaning and micromanipulation capabilities of gecko spatulae and their bio-mimics Nature. Communications **6**, 1 (2015)
19. Zhou, H., Xu, Q., Li, S., Zheng, Y., Wu, X., Gu, C., Chen, Y., Zhong, J.: Dynamic enhancement in adhesion forces of truncated and nanosphere tips on substrates. RSC Adv. **5**(111), 91633 (2015)
20. Li, Q., Dong, Y., Perez, D., Martini, A., Carpick, R.W.: Speed dependence of atomic stick-slip friction in optimally matched experiments and molecular dynamics simulations. Phys. Rev. Lett. **106**, 12 (2011)
21. Kubo, R.: Statistical-mechanical theory of irreversible processes I general theory and simple applications to magnetic and conduction problems. J. Phys. Soc. Jpn. **12**(6), 570 (1957)
22. Kesari, H., Doll, J.C., Pruitt, B.L., Cai, W., Lew, A.J.: Role of surface roughness during hysteresis in adhesive elastic contact. Philos. Mag. Lett. **90**(12), 891 (2010)
23. Carpick, R.W., Salmeron, M.: Scratching the surface: fundamental investigations of tribology with atomic force microscopy. Chem. Rev. **97**(4), 1163 (1997)
24. Szlufarska, I., Chandross, M., Carpick, R.W.: Recent advances in single-asperity nanotribology. J. Phys. D Appl. Phys. **41**(12), 123001 (2008)
25. Maier, S., Sang, Y., Filleter, T., Grant, M., Bennewitz, R., Gnecco, E., Meyer, E.: Fluctuations and jump dynamics in atomic friction experiments. Phys. Rev. B **72**, 24 (2005)
26. Persson, B.N.J., Albohr, O., Tartaglino, U., Volokitin, A.I., Tosatti, E.: On the nature of surface roughness with application to contact mechanics, sealing, rubber friction and adhesion. J. Phys. Condens. Matter **17**(1), R1 (2004)
27. Nikogeorgos, N., Leggett, G.J.: The relationship between contact mechanics and adhesion in nanoscale contacts between non-polar molecular monolayers. Tribol. Lett. **50**(2), 145 (2013)
28. Buzio, R., Valbusa, U.: Probing the role of nanoroughness in contact mechanics by atomic force microscopy. Adv. Sci. Technol. **51**, 90 (2006)
29. Moore, N.W., Houston, J.E.: The pull-off force and the work of adhesion: new challenges at the nanoscale. J. Adhes. Sci. Technol. **24**(15–16), 2531 (2010)
30. Jiang, T., Zhu, Y.: Measuring graphene adhesion using atomic force microscopy with a microsphere tip. Nanoscale **7**(24), 10760 (2015)
31. Jacobs, T.D.B., Lefever, J.A., Carpick, R.W.: Measurement of the length and strength of adhesive interactions in a nanoscale silicon-diamond interface advanced materials. Interfaces **2**(9), 1400547 (2015)